Molecules **2010**, *15*, 8349-8359; doi:10.3390/molecules15118349

OPEN ACCESS

molecules

ISSN 1420-3049

www.mdpi.com/journal/molecules

Article

Synthesis, Structures and Properties of Cu(II) and Mn(II) Complexes with 1,10-Phenanthroline-2-carboxylic acid and 2,2'-Bipyridine Ligands

Jingya Sun * and Huanzhi Xu

College of Marine Sciences, Zhejiang Ocean University, Zhoushan 316000, China;
E-Mail: huanzhixu2009@163.com (H.X.)

* Author to whom correspondence should be addressed; E-Mail: jingyasun2009@163.com;
Tel.: +0086-580-2588934; Fax: +0086-580-2588934.

Received: 10 September 2010; in revised form: 18 October 2010 / Accepted: 25 October 2010 / Published: 15 November 2010

Abstract: Four new 2,2'-bipyridine and 1,10-phenanthroline complexes, namely $[Mn(phenca)_2]\cdot(H_2O)_2$ (**1**), $[Cu_4(phen)_4(OH^-)_4(H_2O)_2](DMF)_4(ClO_4^-)_4(H_2O)$ (**2**), $[Cu_2(2,2\text{-bipy})_2(C_2O_4^{2-})(H_2O)_2(NO_3)_2]$ (**3**) and $[Cu(2,2\text{-bipy})_2(ClO_4^-)](ClO_4^-)$ (**4**) (2,2'-bpy = 2,2'-bipyridine, Hphenca = 1,10-phenanthroline-2-carboxylic acid) have been synthesized by a hydrothermal reaction. The products were characterized by elemental analysis, infrared spectroscopy and X-ray crystal diffraction. While strong hydrogen bonds play central roles in the formation of the 3D structure, the combined influence of the weak interactions such as π···π interactions is also evident in the structures. A preliminary investigation on the ion exchange properties of the complexes is presented.

Keywords: π···π interactions; ion exchange; crystal structure

1. Introduction

Recently, interest in supramolecular chemistry and crystal engineering has been focused on the design strategies and construction of architectures with diversity topologies [1]. One of the most effective strategies is to select organic building blocks with diverse connection modes as directing nodes to assemble multidimensional frameworks by binding metal centers [2].

Self-assembly is the fundamental molecular recognition process adopted by Nature to generate the elegant and intricate molecular machinery from which life is built. Various weak dispersive interactions, such as hydrogen bonds, π···π stacking, hydrophobic charge-transfer, electrostatic as well as metal ion coordination, represent the backbone of self-assembly processes and supramolecular architectures [3]. Aromatic π···π stacking interactions between the π-electron clouds of aromatic systems have been extensively observed in many areas of chemistry and biochemistry [4-10]. They play an essential role in the structures of biological macromolecules such as the double helical structure of DNA, the tertiary structure of proteins and porphyrin aggregation, and are exploited for intercalation of drugs into DNA [11-13].

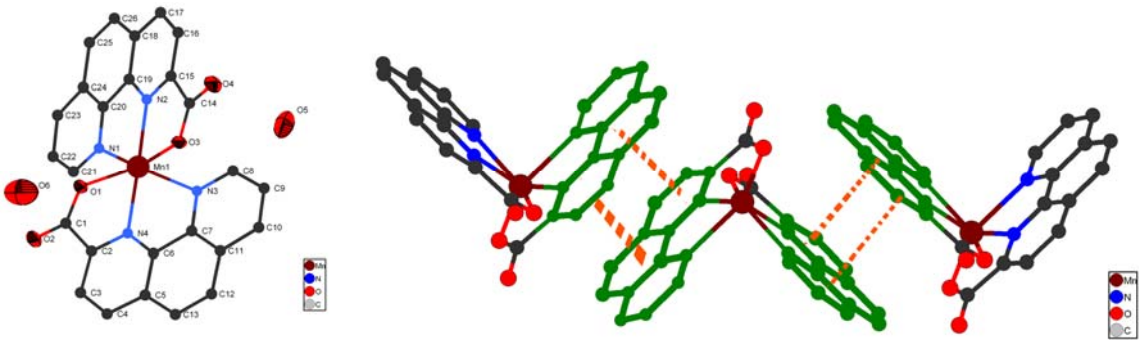
Owing to the strong functionality of π···π stacking interactions, a number of experimental and theoretical methods have been employed to investigate the nature of aromatic-aromatic interaction [14]. Likewise, experimental proofs for carbonyl···π interactions, and more generally for lone pair···π interactions, are presented in the literature [15,16]. Moreover, some molecular architectures, such as helices, cyclophanes and host-guest assemblies, have also been formed through π stacking interactions [17,18]. In this context, we have succeeded in obtaining four novel complexes $[Mn(phenca)_2]$ $(H_2O)_2$ (**1**), $[Cu_4(phen)_4(OH^-)_4(H_2O)_2](DMF)_4(ClO_4^-)_4(H_2O)$ (**2**), $[Cu_2(2,2\text{-bipy})_2(C_2O_4^{2-})(H_2O)_2(NO_3)_2]$ (**3**) and $[Cu\ (2,2\text{-bipy})_2(ClO_4^-)](ClO_4^-)$ (**4**) based on 2,2'-biprydine and 1,10-phenanthroline-2-carboxylic acid ligands. Strong hydrogen bonds and π···π interactions play important roles in the formation of their 3D structures.

2. Results and Discussion

2.1. Crystal structures of compounds **1-4**

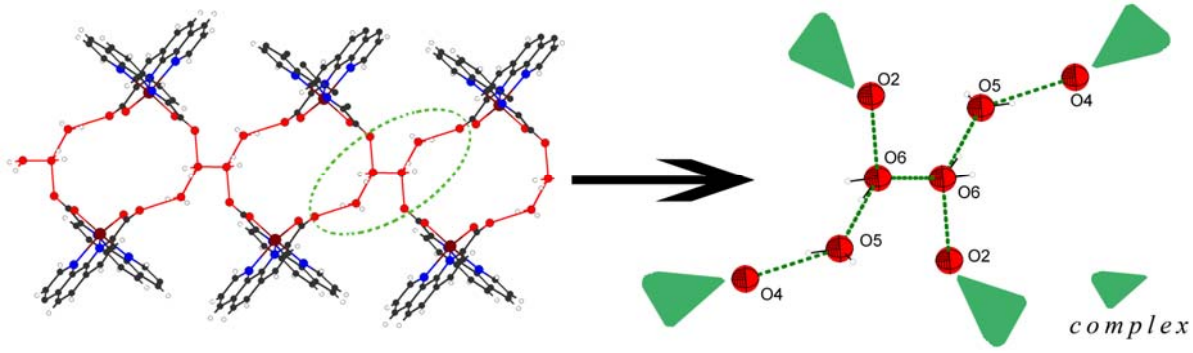
Single-crystal X-ray diffraction measurement reveals that the crystal structure of complex **1** conforms to the space group P-1. A molecular structure showing the arrangement about the Mn (II) metal center is shown in Figure 1(a). The Mn(II) ion is six-coordinated and adopts a distorted octahedron coordination geometry by coordinating to four nitrogen atoms from two phenca ligands (Mn-N(1) 2.440 Å; Mn -N(2) 2.177Å; Mn -N(3) 2.369 Å; Mn -N(4) 2.183 Å) and two oxygen atoms from carboxyl group of the phenca ligand (Mn -O(1) 2.160Å; Mn -O(3) 2.156Å) with N1 and O3 in the axial positions.

Figure 1. (a) The coordination environments of the Mn atom of complex **1** with 30% thermal ellipsolids. **(b)** A perspective view of the π-π stacking interaction between pyridine rings. All the hydrogen atoms are omitted for clarity.



As illustrated in Figure 1(b), stacking interactions play an important role in the formation of the 2D structure [Figure 2(b)]. The adjacent complexes are further connected through face-to-face π-π stacking between pyridine rings (with centroid to centroid distance of 3.644–3.689Å, and an angle of 109°–113°). This interaction is similar to that observed in other recently reported compounds [19,20].

Figure 2. Perspective view of $(H_2O)_4$ morphology in compound **1**. Packing diagram of the supramolecular edifice viewed along the crystallographic b axis, all the hydrogen atoms are omitted for clarity.



It must be remarked that two lattice water molecules and their symmetric equivalents form a $(H_2O)_4$ water cluster and the structure is stabilized by strong hydrogen bonds linking the vertex of the water cluster (Figure 2). All of them are hydrogen bonded through an oxygen atom of a COO group (O4 or O2).

The detailed structure of the water cluster is shown in Figure 2. Carboxyl groups provide potential hydrogen bonding intermolecular interactions, beside its coordination ability towards metal ions. As shown in Figure 2, the O6 adopt triangle distorted geometries with double hydrogen-bond donors, while O5 display single hydrogen-bond donor and acceptor. Within the water cluster, the O···O distances are in range of 2.65(1)–2.88(8) Å with an average of 2.78(5) Å, which is comparable to that observed in the ice II phase 2.77–2.84 Å [21].

Complex **2** conforms to the space group P-1 (Table 1). A molecular structure showing the arrangement about the Cu (II) metal center is shown in Figure 3(a). The Cu atom is five-coordinated and adopts a distorted tetrahedron coordination geometry by coordinating to two nitrogen atoms from the phen ligands and three oxygen atoms from water molecules, with O1 or O3 in the vertex position.

Table 1. Crystal data and structure refinements for complexes **1–4**.

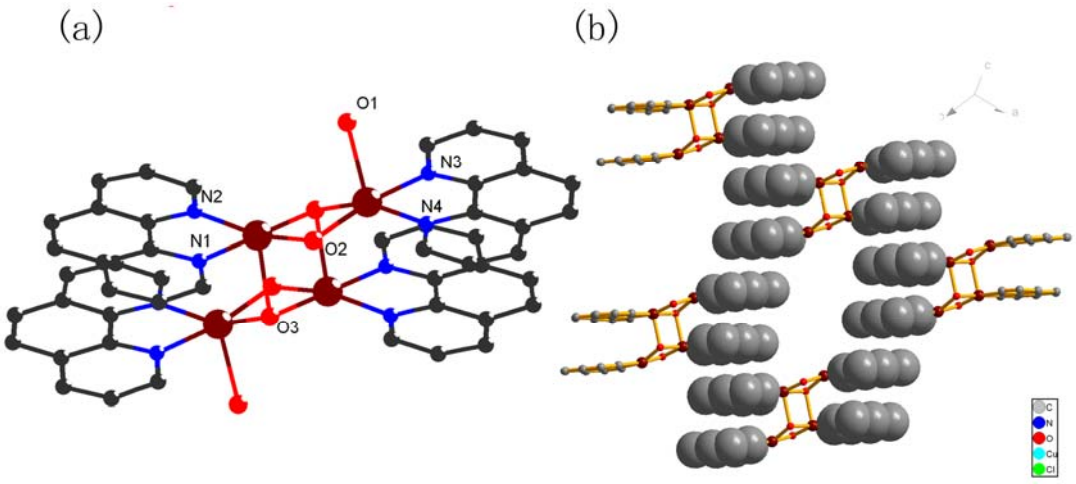
Complexes	**1**	**2**	**3**	**4**
Empirical formula	$C_{26}H_{18}MnN_4O_6$	$C_{60}H_{72}Cl_4Cu_4N_{12}O_{28}$	$C_{22}H_{20}Cu_2N_6O_{12}$	$C_{20}H_{16}Cl_2CuN_4O_8$
Formula mass	537.38	1801.22	687.52	574.81
Temperature(K)	296(2) K	296(2) K	296(2) K	296(2) K
Crystal system	Triclinic	Triclinic	Monoclinic	Triclinic
Space group	p-1	p-1	P2(1)/n	P-1
a(Å)	10.0889(9)	10.1983(18)	7.7035(2)	7.4088(19)
b(Å)	10.5636(9)	14.267(2)	10.2045(3)	11.227(3)
c(Å)	12.1510(10)	15.162(4)	16.5347(5)	14.877(4)
α(°)	71.456(3)	114.261(12)	90	110.164(8)

Table 1. *Cont.*

β(°)	68.256(3)	92.692(11)	100.132(2)	96.489(9)
γ(°)	82.130(4)	110.063(8)	90	99.608(8)
V(Å^3)	1140.13(17)	1843.2(6)	1279.53(6)	1125.7(5)
Z	2	1	2	2
D_{calc}(gcm^{-3})	1.565	1.623	1.784	1.696
μ (mm^{-1})	0.632	1.373	1.740	1.264
F[000]	550		696	582
θ(°)	1.89 to 25.00	1.51 to 25.01	2.36 to 25.01	1.98 to 25.01
Data/restraints/parameters	3943 /0 / 334	920	2259 / 0 / 190	3915 / 0 / 308
Goodness-of-fit on F^2	1.029	1.000	1.096	1.080
Final R[a] indices[I>2σ(I)]	R1 = 0.0624, wR2 = 0.1658	R1 = 0.0627, wR2 = 0.1734	R1 = 0.0267, wR2 = 0.0752	R1 = 0.0777, wR2 = 0.2403
R(int)	0.0457	0.0931	0.0266	0.0272
R indices (all data)	R1 = 0.1232, wR2 = 0.1963	R1 = 0.1358, wR2 = 0.1979	R1 = 0.0325, wR2 = 0.0786	R1 = 0.0883, wR2 = 0.2552

[a] $R_1 = \Sigma(|F_0|-|F_c|)/\Sigma|F_0|$; $wR_2=[\Sigma w(|F_0^2|-|F_c^2)^2/\Sigma w(|F_0^2|^2)]^{1/2}$

Figure 3. (a) The coordination environment of the Cu atoms of complex **2** with 30% thermal ellipsolids. **(b)** The π···π stacking interactions shown in a space filling model.



These complexes are extended through π···π stacking between the phen forming a 2D network (with central to central distance of 3.61–3.63Å). There are 1D channels along the b-axis, and the perchlorate anions are filled into the channels through strong hydrogen bonds as shown in Figure 3(b). It is noteworthy that the perchlorate anion is not coordinated to the 3D framework due to its weak coordination ability.

An ORTEP view of the molecular structure of complex **3** is depicted in Figure 4(a). The selected molecular geometry parameters are listed in Table 2. The Cu(II) ion is six-coordinated and adopts z distorted octahedron coordination geometry by coordinating to two nitrogen atoms from two 2,2'-bipyridine ligands (Cu-N(1) 1.969Å; Cu-N(2) 1.984Å) and four oxygen atoms from an oxalic acid molecule, a coordinated water molecule and nitrate ion (Cu-O(1) 1.9700 Å; Cu-O(2) 1.9864 Å; Cu-O(3) 2.344 Å; Cu-O(4) 2.761Å) with O3 and O4 in the axial positions.

Figure 4. (a) The coordination environment of the centeral metal ions of complex **3** with 50% thermal ellipsoids. **(b)** A perspective view of the π-π stacking interaction between 2,2'-pyridine rings. **(c)** Packing diagram connected by hydrogen bonding. All hydrogen atoms are omitted for clarity.

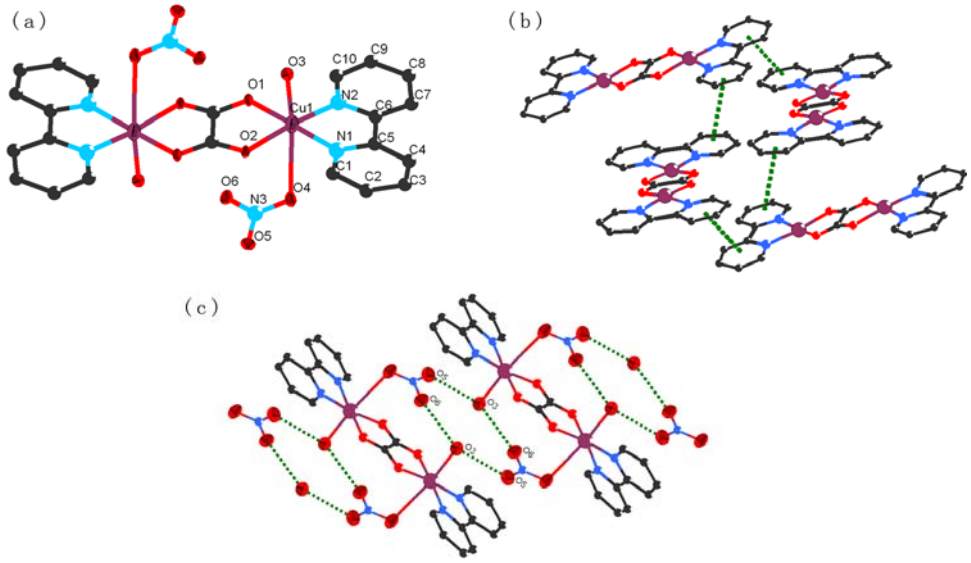


Table 2. Selected bond lengths (Å) and angles (°) for complexes **1-4**.

Complex 1			
Mn(1)-O(3)	2.156(4)	Mn(1)-N(2)	2.177(4)
Mn(1)-O(1)	2.160(4)	Mn(1)-N(4)	2.183(4)
Mn(1)-N(3)	2.370(5)	Mn(1)-N(1)	2.440(4)
O(3)-Mn(1)-O(1)	105.32(16)	O(3)-Mn(1)-N(2)	73.80(15)
O(1)-Mn(1)-N(2)	118.99(16)	O(3)-Mn(1)-N(4)	127.70(15)
O(1)-Mn(1)-N(4)	73.27(17)	N(2)-Mn(1)-N(4)	153.89(17)
O(3)-Mn(1)-N(3)	92.17(15)	O(1)-Mn(1)-N(3)	143.85(16)
N(2)-Mn(1)-N(3)	96.02(16)	N(4)-Mn(1)-N(3)	71.02(16)
O(3)-Mn(1)-N(1)	143.97(15)	O(1)-Mn(1)-N(1)	92.31(15)
N(2)-Mn(1)-N(1)	70.16(16)	N(4)-Mn(1)-N(1)	87.16(16)
N(3)-Mn(1)-N(1)	91.40(15)		
Complex 2			
Cu(1)-O(2)	1.919(4)	Cu(1)-O(3)#1	1.971(4)
Cu(1)-N(1)	2.023(5)	Cu(1)-N(2)	2.035(4)
Cu(1)-O(3)	2.335(4)	Cu(1)-Cu(2)	2.9347(9)
Cu(2)-O(2)	1.937(4)	Cu(2)-O(3)#1	1.973(3)
Cu(2)-N(4)	2.016(5)	Cu(2)-N(3)	2.030(5)
Cu(2)-O(1)	2.250(5)	O(3)-Cu(1)#1	1.971(4)
O(3)-Cu(2)#1	1.973(3)	O(2)-Cu(1)-O(3)#1	81.55(15)
O(2)-Cu(1)-N(1)	96.60(17)	O(3)#1-Cu(1)-N(1)	178.04(16)
O(2)-Cu(1)-N(2)	164.89(18)	O(3)#1-Cu(1)-N(2)	100.31(17)
N(1)-Cu(1)-N(2)	81.30(18)	O(2)-Cu(1)-O(3)	97.81(16)
O(3)#1-Cu(1)-O(3)	86.15(15)	N(1)-Cu(1)-O(3)	94.79(17)
N(2)-Cu(1)-O(3)	97.28(15)	O(2)-Cu(1)-Cu(2)	40.68(11)
O(2)-Cu(2)-O(3)#1	81.05(15)	O(2)-Cu(2)-N(4)	95.43(19)

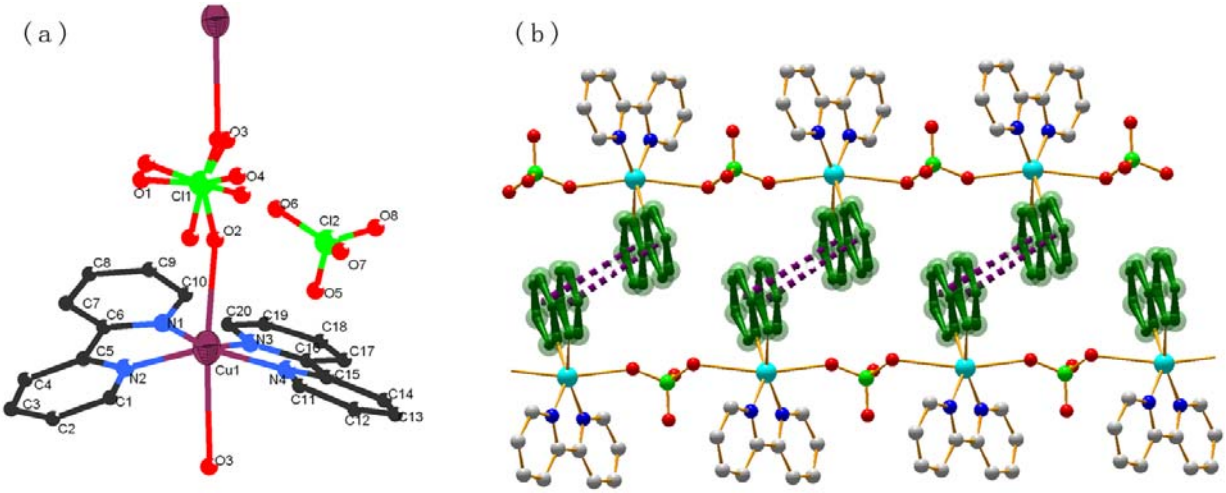
Table 2. *Cont.*

O(3)#1-Cu(2)-N(4)	156.91(19)	O(2)-Cu(2)-N(3)	171.42(19)
O(3)#1-Cu(2)-N(3)	98.89(18)	N(4)-Cu(2)-N(3)	81.2(2)
O(2)-Cu(2)-O(1)	96.55(18)	O(3)#1-Cu(2)-O(1)	101.24(17)
N(4)-Cu(2)-O(1)	101.83(19)	N(3)-Cu(2)-O(1)	91.88(19)
Symmetry transformations used to generate equivalent atoms: #1 -x+1,-y+1,-z+1			
Complex 3			
Cu(1)-O(1)	2.0135(18)	N(1)-Cu(1)-N(4)	97.27(10)
Cu(1)-N(3)	2.018(2)	O(1)-Cu(1)-N(2)	93.09(8)
Cu(1)-N(1)	2.036(2)	N(3)-Cu(1)-N(2)	98.90(9)
Cu(1)-N(4)	2.041(2)	N(1)-Cu(1)-N(2)	77.45(9)
Cu(1)-O(1)	2.0135(18)	N(4)-Cu(1)-N(2)	99.83(9)
Cu(1)-O(2)#1	2.325(2)	O(1)-Cu(1)-O(2)#1	76.85(7)
O(1)-Cu(1)-N(3)	92.97(9)	N(3)-Cu(1)-O(2)#1	88.32(9)
O(1)-Cu(1)-N(1)	90.37(8)	N(1)-Cu(1)-O(2)#1	95.82(9)
N(3)-Cu(1)-N(1)	175.19(8)	N(4)-Cu(1)-O(2)#1	90.83(8)
O(1)-Cu(1)-N(4)	166.14(9)	N(2)-Cu(1)-O(2)#1	167.98(8)
N(3)-Cu(1)-N(4)	80.18(10)		
Symmetry transformations used to generate equivalent atoms: #1 -x+1,-y+2,-z+1			
Complex 4			
Cu(1)-N(3)	1.973(6)	N(1)-Cu(1)-N(4)	103.5(2)
Cu(1)-N(1)	1.984(5)	N(2)-Cu(1)-N(4)	151.9(2)
Cu(1)-N(2)	1.994(5)	N(3)-Cu(1)-N(2)	102.2(2)
Cu(1)-N(4)	1.995(6)	N(1)-Cu(1)-N(2)	81.7(2)
N(3)-Cu(1)-N(1)	160.9(2)	N(3)-Cu(1)-N(4)	81.9(3)

In the crystal structure of **3**, the oxalic acid acts as the bridge ligand which links two copper atoms, while two 2,2'-bipy molecules act as terminal ligands on each side. Analysis of the crystal packing of the title compound reveals the existence of multiple intermolecular π-π stacking interaction (with an average centroid-to-centroid distance of 3.923Å) between the 2,2'-bipyridine molecules, forming a two-dimensional sheet [Figure 4(b)]. In addition, O-H-O hydrogen bonds play important roles in the formation of the 2D structure, in which O3 acts as double hydrogen-bond donors towards O5 and O6 of the nitrate ion [Figure 4(c)].

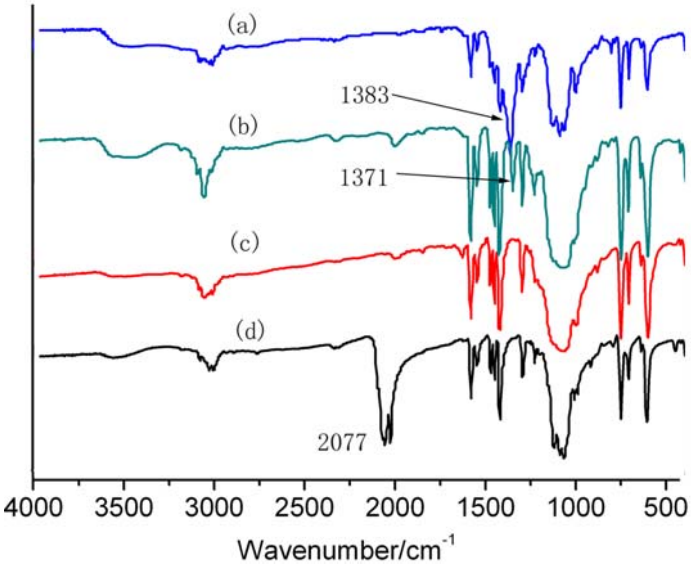
Single-crystal X-ray diffraction measurement reveals that the crystals of complex **4** conform to the space group P-1. A molecular structure showing the arrangement about the Cu (II) mental center is shown in Figure 5(a). The structure consists of a polymeric three-dimensional network in which each metal atom is six-coordinated and adopts a distorted octahedron coordination geometry by coordinating to four nitrogen atoms from two 2,2'-bipyridine molecules (Cu-N(1) 1.984Å; Cu-N(2) 1.994Å; Cu-N(3) 1.973Å; Cu-N(4) 1.995Å) lie on the equatorial plane and two oxygen atoms from the perchlorate anion Cu-O(2) 2.490 Å; Cu-O(2) 2.742 Å) in the axial positions. The structure is expanded into a chain along a axis by using the perchlorate anion as a bridge ligand. The chains are further extended by the π-π stacking interactions between the adjacent 2,2'-bipyridine molecules to form a 3D structure. In this structure, the terminal pyridyl rings are overlapped with a centroid-to-centroid distance of 3.62 to 3.96 Å.

Figure 5. (a) The coordination environment of the Cu atoms of complex **4** with 30% thermal ellipsolids. **(b)** A perspective view of the π-π stacking interaction between pyridine rings. All the hydrogen atoms are omitted for clarity.



As revealed by the crystal structure analysis of complex **4**, the perchlorate anions are located within the open structure of the 1D channel through C-H-O hydrogen bond and π-π stacking interactions (Figures 5). Complex **4** is expected to display anion exchange properties since it is insoluble in common solvents. The FT-IR and XRD spectra of the exchanged product and the original **4** are shown in Figures 6 and Figure s6, respectively. Characteristic intense bands appear about 1,383 cm^{-1}, which originate from the NO_3^- ion [22], while the characteristic intense bands in the range from 2,077 to 2,130 cm^{-1} originate from the SCN^- ion [23,24]. Furthermore, the elemental analysis result also indicated anion exchange, but the exchange was incomplete.

Figure 6. FT-IR spectra of **(a)** complex **4** treated with aqueous solution of $NaNO_3$, **(b)** complex **4** treated with aqueous solution of $NaNO_2$, **(c)** complex **4**, **(d)** complex **4** treated with aqueous solution of KSCN.



TGA (Figures s1- s4) were carried out in the interest of studying the thermal behavior of complexes **1-4**. We selected complex **1** as an example to study the thermal behavior. The TGA indicates that **1** loses 6.7% of total weight in the 30–90 °C temperature range, corresponding to the removal of two lattice water molecules per formula unit (calcd. 6.7%). When the temperature continues rising, the products lose 83% of the total weight in the 200–300 °C temperature range, corresponding to the removal of the phenca ligand (Figure s1). Complexes **2-4** also display good thermal stability.

3. Experimental

3.1. Materials and Physical Measurements

All chemicals were commercial materials of analytical grade and used without further purification. FT-IR spectra were recorded on a Nicolet Magna-IR 550 spectrometer in dry KBr pellets. C, H and N analysis was measured on a MOD 1106 elemental analyzer. The PXRD data were collected on a Bruker D8 diffractometer with Cu Kα radiation (λ = 1.5418Å).

3.2. Synthesis of **1-4**

3.2.1. Synthesis of $[Mn(phenca)_2](H_2O)_2$ (**1**)

A solution of phenca (0.224 g, 1 mmol) and $Mn(CH_3COO)_2$ (0.172 g, 1 mmol) in water (10 mL) was stirred for 30 min at room temperature. Slow evaporation of the solvent at room temperature led to the formation of yellow block crystals of **1**. Yield: 68% (based on Mn). Anal. Calcd for $C_{26}H_{18}MnN_4O_6$ (%): C, 58.11; H, 3.38; N, 10.43. Found: C, 58.12; H, 3.37; N, 10.41. IR (cm^{-1}): 3,300, 1,685 m (v C=O), 1,585 (v C=N) 1,510, 1,305 s, 849 s.

3.2.2. Synthesis of $[Cu_4(phen)_4(OH^-)_4(H_2O)_2](DMF)_4(ClO_4^-)_4(H_2O)$ (**2**)

A solution of phen (0.18 g, 1 mmol) and $Cu(ClO_4)_2$ (0.152 g, 1 mmol) in DMF/H_2O (10 mL, 1:1) was stirred for 10 min at room temperature and placed in a 25 mL Teflon-lined autoclave and heated at 150 °C for 120 h. The autoclave was cooled over a period of 8 h at 10 °C h^{-1}, and compound **2**, obtained as blue block crystals, was collected by filtration, and dried at ambient temperature. Yield: 59% (based on Cu). Anal. Calcd for $C_{60}H_{72}Cl_4Cu_4N_{12}O_{28}$ (3): C, 40.01; H, 3.81; N, 9.33. Found (%): C, 40.79; H, 4.02; N, 9.25. IR (cm^{-1}): 3,420, 1,695m (v C=O), 1,575 (v C=N), 1,110.

3.2.3. Synthesis of $[Cu_2(2,2\text{-bipy})_2(C_2O_4^{2-})(H_2O)_2(NO_3)_2]$ (**3**)

A solution of 2,2'-bipyridine (0.312 g, 2 mmol) and $Cu(NO_3)_2$ (0.241 g, 1 mmol) in DMF (10 mL) was slowly added to a solution of oxalic acid (0.180 g, 2mmol) in DMF (10 mL). The mixture was stirred for 10 min at 298 K and then placed in a 25 mL Teflon-lined autoclave and heated at 150 °C for 120 h. The autoclave was cooled over a period of 8 h at 10 °C h^{-1}, and **3** was collected as blue block crystals by filtration, and dried at ambient temperature. Yield: 60% (based on Cu). Anal. Calcd for $C_{22}H_{20}Cl_2Cu_2N_6O_{12}$ (1): C, 48.29; H, 3.90; N, 11.60. Found (%): C,48.65; H, 3.91; N, 11.82. IR (cm^{-1}): 3,320, 1,692 m (v C=O), 1,563 (v C=N), 1,380, 856.

3.2.4. Synthesis of [Cu (2,2-bipy)$_2$(ClO_4^-)](ClO_4^-) (**4**)

A solution of 2,2'-bipyridine (0.156 g, 1 mmol) and $Cu(ClO_4)_2$ (0.076 g, 0.5 mmol) in ethanol (10 mL) was stirred for 10 min at room temperature and then placed in a 25 mL Teflon-lined autoclave and heated at 150 °C for 120 h. The autoclave was cooled over a period of 8 h at 10 °C h^{-1}, and **4** was collected by filtration as blue block crystals, that were dried at ambient temperature. Yield: 60% (based on Cu). Anal. Calcd for $C_{20}H_{16}Cl_2CuN_4O_8$ (3): C, 41.29; H, 2.80; N, 9.60. Found (%): C, 41.79; H, 2.81; N, 9.75. IR (cm^{-1}): 1,670m (v C=O), 1,480, 1,110, 656.

3.3. Single-crystal Structure Determination

Intensity data for 1-4 were collected at 296 K on a Bruker SMART CCD area detector diffractometer using graphite-monochromated Mo-Kα radiation (λ = 0.71073 Å) using the *ω-θ* scan mode in the range $1.51 \leq \theta \leq 25.01°$. Raw frame data were integrated with the SAINT [25] program. The structure was solved by direct methods using SHELXS-97 and refined by full-matrix least-squares on F^2 using SHELXS-97 [26]. An empirical absorption correction was applied with SADABS [26]. All non-hydrogen atoms were refined anisotropically. Hydrogen atoms were set in calculated positions and refined by a riding mode, with a common thermal parameter. All calculations and graphics were performed with SHELXTL [25] and DIAMOND. The crystallographic data and experimental details for the structure analysis are summarized in Table 1.

4. Conclusions

In conclusion, we have prepared and characterized four complexes: $[Mn(phenca)_2](H_2O)_2$ (**1**), $[Cu_4(phen)_4(OH^-)_4(H_2O)_2](DMF)_4(ClO_4^-)_4(H_2O)$ (**2**), $[Cu_2(2,2\text{-bipy})_2(C_2O_4^{2-})(H_2O)_2(NO_3)_2]$ (**3**) and [Cu(2,2-bipy)$_2$(ClO_4^-)](ClO_4^-) (**4**) and determined their crystal structures. Hydrogen bonding, π···π stacking interactions and cation···π interactions are found to form the packing structure. The complexes also display strong thermal stability.

Supplementary Materials

Supplementary materials can be found at http://www.mdpi.com/1420-3049/15/11/8349/s1.

Acknowledgements

The authors thank the Project Supported by Scientific Research Fund of Zhejiang Provincial Education Department (y200908138).

References and Notes

1. Chui, S.S.; Lo, S.M.F.; Charmant, J.P.H.; Orpen, A.G.; I.D. Williams. A Chemically Functionalizable Nanoporous Material $[Cu_3(TMA)_2(H_2O)_3]$n. *Science* **1999**, *283*, 1148-1150.
2. Leininger, S.; Olenyuk, B.; Stang, P.J. Self-Assembly of Discrete Cyclic Nanostructures Mediated by Transition Metals. *Chem. Rev*. **2000**, *100*, 853-908.

3. Biradha, K.; Zaworotko, M.J. A Supramolecular Analogue of Cyclohexane Sustained by Aromatic C−H···π Interactions: Complexes of 1,3,5-Trihydroxybenzene with Substituted Pyridines. *J. Am. Chem. Soc.* **1998**, *120*, 6431-6432.
4. Cockroft, S.L.; Hunter, C.A.; Lawson, K.R.; Perkins, J.; Urch, C.J. Electrostatic Control of Aromatic Stacking Interactions. *J. Am. Chem. Soc.* **2005**, *127*, 8594-8595.
5. Cheruzel, L.E.; Mashuta, M.S.; Buchanan, R.M. A supramolecular assembly of side-by-side polyimidazole tripod coils stabilized by π–π stacking and unique boric acid templated hydrogen bonding interactions. *Chem. Commun.* **2005**, 2223-2225.
6. Chipot, C.; Jaffe, R.; Maigret, B.; Pearlman, D.A.; Kollman, P.A. Benzene Dimer: A Good Model for π−π Interactions in Proteins? A Comparison between the Benzene and the Toluene Dimers in the Gas Phase and in an Aqueous Solution. *J. Am. Chem. Soc.* **1996**, *118*, 11217-11224.
7. Pletneva, E.V.; Laederach, A.T.; Fulton, D.B.; Kostić, N.M. The Role of Cation−π Interactions in Biomolecular Association. Design of Peptides Favoring Interactions between Cationic and Aromatic Amino Acid Side Chains. *J. Am. Chem. Soc*. **2001**, *123*, 6232-6245.
8. Meyer, E.A.; Castellano, R.K.; Diederich, F. Interactions with Aromatic Rings in Chemical and Biological Recognition. *Angew. Chem. Int. Ed.* **2003**, *42*, 1210-1250.
9. Alcock, N.W.; Barker, P.R.; Haider, J.M.; Hannon, M.J.; Painting, C.L.; Plummer, E.A.; Rissanen, K.; Saarenketo, P. Red and blue luminescent metallo-supramolecular coordination polymers assembled through π–π interactions. *J. Chem. Soc. Dalton Trans.* **2000**, 1447-1462.
11. Saenger, W. *Principles of Nucleic Acid Structure*; Springer-Verlag: NewYork, NY, USA, 1984; pp.132-135.
12. Nohra, B.; Yao, Y.; Lescop, C.; Réau, R. Coordination Polymers with π -Stacked Metalloparacyclophane Motifs: F-Shaped Mixed-Coordination Dinuclear Connectors. *Angew. Chem. Int. Ed.* **2007**, *46*, 8242-8245.
13. Sauvage, J.P.; Collin, J.P.; Chambron, J.C.; Guillerez, S.; Coudret, C. Ruthenium(II) and Osmium(II) Bis(terpyridine) Complexes in Covalently-Linked Multicomponent Systems: Synthesis, Electrochemical Behavior, Absorption Spectra, and Photochemical and Photophysical Properties. *Chem.Rev*. **1994**, *94*, 993-1019.
14. Egli, M.; Sarkhel, S. Lone Pair−Aromatic Interactions: To Stabilize or Not to Stabilize. *Acc. Chem. Res*. **2007**, *40*, 197-205.
15. Mooibroek, T.J.; Teat, S.J.; Massera, C.; Gamez, P.; Reedijk, J. Crystallographic and Theoretical Evidence of Acetonitrile−π Interactions with the Electron-Deficient 1,3,5-Triazine Ring. *Cryst. Growth Des.* **2006**, *6*, 1569-1574.
16. Chas, M.; Blanco, V.; Peinador, C.; Quintela, J.M. Synthesis of [3]Catenanes Based on Metal-Directed Self-Assembly and π-Donor/π-Acceptor Interactions. *Org. Lett.* **2007**, *9*, 675-678.
17. Munakata, M.; Wu, L.P.; Kuroda-Sowa, T.; Maekawa, M.; Suenaga, Y.; Ning, G.L.; Kojima, T. Supramolecular Silver(I) Complexes with Highly Strained Polycyclic Aromatic Compounds. *J. Am. Chem. Soc*. **1998**, *120*, 8610-8618.
18. Paul, R.L.; Couchman, S.M.; Jeffery, J.C.; McCleverty, J.A.; Reeves, Z.R.; Ward, M.D. Effects of metal co-ordination geometry on self-assembly: A dinuclear double helicate complex and a tetranuclear cage complex of a new bis-bidentate bridging ligand. *J. Chem. Soc. Dalton Trans.* **2000**, 845-851.

19. Liu, Y.Y.; Ma, J.F.; Yang, J.; Ma, J.C.; Su, Z.M. Versatile frameworks constructed from divalent metals and 1,2,3,4-butanetetracarboxylate anion: Syntheses, crystal structures, luminescence and magnetic properties. *Cryst. Eng. Comm.* **2008**, *10*, 894-904.
20. Bondar, O.A.; Lukashuk, L.V.; Lysenko, A.B.; Krautscheid, H.; Rusanov, E.B.; Chernega, A.N.; Domasevitch, K.V. New microporous copper(II) coordination polymers based upon bifunctional 1,2,4-triazole/tetrazolate bridges . *Cryst. Eng. Comm.* **2008**, *10*, 1216-1226.
21. Gregory, J.K.; Clary, D.C.; Liu, K.; Brown, M.G.; Saykally, R.J. The Water Dipole Moment in Water Clusters. *Science* **1997**, *275*, 814-817.
22. Su, Z.; Bai, Z.S.; Xu, J.; Okamura, T.; Liu, G.X.; Chu, Q.; Wang, X.F.; Sun, W.Y.; Ueyama, N. Synthesis, structure and property of cobalt(II) complexes with 3,5-di(1H-imidazol-1-yl)benzoic acid. *Cryst. Eng. Comm.* **2009**, *11*, 873-880.
23. Sun, J.; Tong, X.; Xu, H. Synthesis, structures and properties of Cu and Cd complexes with 1,10-phenanthroline. *Inorg. Chem. Commun.* **2010**, *13*, 645-648.
24. Sun, J.; Tong, X. Aqua(6,6'-oxydipicolinato-κ^2*O*,*N*,*N*',*O*')copper(II). *Acta Cryst.* 2010, E**66**, m70.
25. Siemens. *SAINT: Area Detector Control and Integration Software*. Siemens Analytical X-ray Instruments Inc.: Madison, WI, USA, 1996.
26. Sheldrick, G.M. *SHELXL97 and SHELXTL Software Reference Manual, Vol. 5.1*.; Bruker AXS Inc.: Madison, WI, USA, 1997.
27. Crystallographic data (excluding structure factors) for the structures in this paper have been deposited with the Cambridge Crystallographic Date Centre as supplementary publications CCDC 776482，776483，770153 and 770155 for 1-4, respectively. Copies of the data can be obtained free of charge on application to CCDC, 12 Union Road, Cambridge CB2 1EZ, UK [Fax: 441223-336-033; Email: deposit@ccdc.cam.ac.uk.]

Sample Availability: Contact the authors.

© 2010 by the authors; licensee MDPI, Basel, Switzerland. This article is an open access article distributed under the terms and conditions of the Creative Commons Attribution license (http://creativecommons.org/licenses/by/3.0/).